Hydrogen Exchange Behavior of [U − 15 N]-Labeled Oxidized and Reduced Iso-1-cytochrome c †

ARTICLE *in* BIOCHEMISTRY · MAY 1999

Impact Factor: 3.02 · DOI: 10.1021/bi982742z · Source: PubMed

2 AUTHORS:

Susan M Baxter
California State University, Chancellor's Office
23 PUBLICATIONS **563** CITATIONS

SEE PROFILE

Jacquelyn Fetrow
University of Richmond
87 PUBLICATIONS **2,943** CITATIONS

SEE PROFILE

Hydrogen Exchange Behavior of [*U*-^{15}N]-Labeled Oxidized and Reduced Iso-1-cytochrome *c*[†]

Susan M. Baxter[‡] and Jacquelyn S. Fetrow*[,§]

Wadsworth Center and Department of Biomedical Sciences, New York State Department of Health, Empire State Plaza, Albany, New York 12201-0509, and Department of Molecular Biology, The Scripps Research Institute, 10550 North Torrey Pines Drive, La Jolla, California 92037

Received November 18, 1998; Revised Manuscript Received January 27, 1999

ABSTRACT: Heteronuclear NMR spectroscopy was used to measure the hydrogen−deuterium exchange rates of backbone amide hydrogens in both oxidized and reduced [*U*-^{15}N]iso-1-cytochrome *c* from the yeast *Saccharomyces cerevisiae.* The exchange data confirm previously reported data [Marmorino et al. (1993) *Protein Sci. 2*, 1966−1974], resolve several inconsistencies, and provide more thorough coverage of exchange rates throughout the cytochrome *c* protein in both oxidation states. Combining the data previously collected on unlabeled C102T with the current data collected on [*U*-^{15}N]C102T, exchange rates for 53 protons in the oxidized state and 52 protons in the reduced state can now be reported. Most significantly, hydrogen exchange measurements on [*U*-^{15}N]iso-1-cytochrome *c* allowed the observation of exchange behavior of the secondary structures, such as large loops, that are not extensively hydrogen-bonded. For the helices, the most slowly exchanging protons are found in the middle of the helix, with more rapidly exchanging protons at the helix ends. The observation for the Ω-loops in cytochrome *c* is just the opposite. In the loops, the ends contain the most slowly exchanging protons and the loop middles allow more rapid exchange. This is found to be true in cytochrome *c* loops, even though the loop ends are not attached to any regular secondary structures. Some of the exchange data are strikingly inconsistent with data collected on the C102S variant at a different pH, which suggests pH-dependent dynamic differences in the protein structure. This new hydrogen exchange data for loop residues could have implications for the substructure model of eukaryotic cytochrome *c* folding. Isotopic labeling of variant forms of cytochrome *c* can now be used to answer many questions about the structure and folding of this model protein.

Cytochromes *c* are small proteins that function as electron carriers between the last two complexes in the electron transport chains of eukaryotic organisms (*1*). These proteins are globular and contain a heme prosthetic group. The heme group is responsible for accepting a single electron from complex III (cytochrome *c* reductase) and carrying that electron to complex IV (cytochrome *c* oxidase) (*1*). In shuttling the electron between complexes III and IV, the iron in the heme group alternates between the reduced, diamagnetic form, Fe(II), and the oxidized, paramagnetic form, Fe(III). The heme group is thus responsible for the electron-transfer function of the cytochromes *c*, and the protein itself is responsible for maintaining the redox state of the iron in the aqueous cellular environment and for recognizing and docking to the appropriate redox partners.

Cytochromes *c* are good models for studying protein folding and structure/function relationships. These proteins undergo a reversible, two-state denaturation and many different techniques have been used to analyze their folding pathways (see, for example, refs *2*−*10*). High-quality structures for eukaryotic cytochromes *c* from a number of wild-type and variant proteins have been determined by X-ray crystallography and NMR spectroscopy (see, for example, refs *11*−*21*). The sequences of over 100 eukaryotic cytochromes *c* are known and the proteins from these organisms are quite similar, including similar overall structures and many evolutionarily invariant residues throughout the sequences (*22*).

Hydrogen exchange experiments monitored by NMR spectroscopy are used, among other things, to study the dynamics and equilibrium behavior of proteins. These experiments allow site-specific probes of the backbone dynamics throughout a protein. Previously, hydrogen exchange data had been collected and rate constants calculated for a subset of residues in the unlabeled C102T variant of yeast iso-1-cytochrome *c* (*23*) and for cytochrome *c* from horse heart (*9*, *24*−*27*). Exchange behavior of amide protons in the unlabeled C102S variant from yeast was also reported, but data from only a few time points were collected so no rate constants were calculated (*17*, *19*). Hydrogen exchange experiments on C102T found slowly exchanging protons both in the hydrogen-bonded helices and in the nonregular, Ω-loop regions of the protein (*23*). These researchers also showed that reduction of the heme group in the protein results in a

[†] This work was partially supported by NIH Grant GM44829 to J.S.F.

* To whom correspondence should be addressed at Department of Molecular Biology, Mail TPC5, The Scripps Research Institute, 10550 North Torrey Pines Dr., La Jolla, CA 92037; phone 619-784-8830; fax 619-784-8895; email jacque@scripps.edu.

[‡] New York State Department of Health.

[§] The Scripps Research Institute.

10.1021/bi982742z CCC: $18.00
Published on Web 03/17/1999

general increase in the free energy for the local unfolding reactions (ΔG_{op}) that can result in hydrogen exchange.

Up to this time, NMR studies of eukaryotic cytochromes *c* have been limited to work on unlabeled proteins. While the heme group in cytochrome *c* provides some peak dispersion in the proton spectra, ^{15}N labeling provides an additional dimension of resolution. Use of unlabeled protein also limits the time scale for hydrogen exchange experiments. An HSQC spectrum on [*U*-^{15}N]-labeled protein can be collected much more rapidly than a COSY or TOCSY spectrum on an unlabeled, but otherwise identical, protein. To overcome the limitations of working with an unlabeled cytochrome *c*, we have developed a method to isotopically label iso-1-cytochrome *c* expressed in yeast. Preliminary results of hydrogen exchange experiments on [*U*-^{15}N]C102T describing the analysis of the C-helix have been published (*28*). The accompanying paper describes in detail the method for producing [*U*-^{15}N]iso-1-cytochrome *c*, presents the ^{1}H and ^{15}N assignments for both oxidized and reduced states of the protein, and analyzes the ^{15}N relaxation data for both of these states (*29*).

In this paper, we present hydrogen exchange rates for backbone amide protons in both oxidized and reduced [*U*-^{15}N]iso-1-cytochrome *c*. For those rates that could be measured in both labeled and unlabeled protein, these data correlate well with the previously published hydrogen exchange data on unlabeled iso-1-cytochrome *c* (*23*) and resolve some discrepancies in the previous analysis. More significantly, ^{15}N-labeling of the protein allows us to observe protons that exchange more quickly than could be observed in previous experiments. With greater coverage of the protein, we can study in more detail the hydrogen exchange behavior of the non-hydrogen-bonded secondary structures, such as Ω-loops, some of which are thought to be important in biological activity, in this eukaryotic cytochrome *c*. These data provide a more thorough evaluation and understanding of the backbone dynamics of this model globular protein.

MATERIALS AND METHODS

Yeast Strains and Proteins. Yeast strain C93 (*30*) produces C102T, the iso-1-cytochrome *c* variant in which the cysteine at position 102 is replaced by threonine. This variant does not dimerize through intermolecular disulfide bonds and this facilitates in vitro analysis of the protein. Its properties are virtually identical to those of true wild-type iso-1-cytochrome *c* (*31, 32*) and it has been used as the "wild type" by us (*33*) and others (*23, 34, 35*). Iso-1-cytochrome *c* contains five extra residues at the amino terminus when aligned with other eukaryotic cytochromes *c*; thus, we follow the convention of numbering its residues from −5 to 103.

Yeast Fermentation and Purification of Isotopically [U-^{15}N]-Labeled C102T. Fermentation and purification of complete [*U*-^{15}N]C102T was done as described in the accompanying paper (*29*). To produce the data described in this paper, two 7-L batches of C93 were grown in ^{15}N-labeled minimal medium. The yield of protein from each batch was about 2−3 mg. Cells were harvested and C102T was purified by a modification (*33*) of the standard two ion-exchange column protocol (*36*). Protein was oxidized with $K_3Fe(CN)_6$, and the $K_3Fe(CN)_6$ was removed by use of a small Sephadex DEAE A25 column prior to the second ion-exchange column. Following the second ion-exchange column and dialysis into NMR buffer (50 mM deuterated acetate in H_2O, pH 4.6), the protein was slowly concentrated through Centricon filters. The protein was not lyophilized. Protein composition was confirmed by high-performance liquid chromatography (HPLC)−electron spray ionization (LC-ESI) mass spectroscopy. The molecular weight of [*U*-^{15}N]C102T was found to be 12 858, as expected for complete ^{15}N labeling of C102T.

NMR Sample Preparation and Exchange into D_2O. Previous experience with cytochrome *c* samples has shown that dissolution of lyophilized protein into buffer results in minor, but significant, populations of misfolded and poorly behaved protein for NMR studies (J.S.F. and S.M.B., unpublished observations). Consequently, the protein was not lyophilized for these labeled samples but was concentrated to a volume of about 500 μL, as described above, and exchanged into D_2O by use of Sephadex G25 spin columns. G25 resin was swelled and equilibrated in 50 mM deuterated acetate, pH 4.6 (uncorrected), prepared in D_2O. Following overnight equilibration at 4 °C, 10 mL of G25 resin was poured into a disposable column and spun in an IEC benchtop clinical centrifuge at 1500*g* relative centrifugal field for about 1 min to dry the resin. Acetate D_2O buffer (500 μL) was applied to the top of the column and spun for 30 s at 1500*g* to check volume recovery and to wash the column. The aqueous protein sample was then applied to the top of the column and the column was spun for 40 s at 1500*g* to recover the labeled protein sample, now exchanged into D_2O. About 5% of the sample was lost during this exchange protocol. For experiments on reduced protein samples, the exchange buffer contained 12 mM ascorbate to help maintain a reducing environment. To reduce the sample immediately prior to exchange, a few grains of dithionite were added to the protein solution.

Following exchange, 2 μL of the protein sample was removed to determine the protein concentration using visible absorbance spectroscopy. An extinction coefficient of 106.1 mM^{-1} cm^{-1} (*37, 38*) at 410 nm was used to determine protein concentrations of 0.22 mM for oxidized C102T and 0.21 mM for reduced C102T NMR samples. The remaining sample from the exchange column was loaded into an NMR tube for immediate analysis. To correlate easily with previous chemical shifts reported for yeast C102T (*23*), dioxane was added to the NMR samples as an internal chemical shift standard.

Nuclear Magnetic Resonance Spectroscopy. [^{1}H−^{15}N] HSQC spectra were recorded at 298 K on a Bruker Avance DRX500 spectrometer. Water suppression by WATERGATE pulses (*39*) was incorporated into the HSQC pulse sequence. Frequency jumping was used to shift the transmitter to the center of the amide region of the proton spectrum. States-TPPI phase cycling was used in the nitrogen dimension. Relaxation time between scans was 1.5 s. Each HSQC experiment was acquired in 28.5 min.

For oxidized C102T, the data sets consisted of 64 t_1 increments, eight scans for each, and 2K points in t_2. The spectral width in the proton dimension was 2155 Hz; the spectral width in the nitrogen dimension was 1800 Hz. Acquisition of the first spectrum was complete at 46.85 min and the remaining spectra were collected consecutively for 1385.8 min (28.5 min/acquisition). For reduced C102T, the data sets consisted of 64 t_1 increments, eight scans for each,

and 1K points in t_2. The spectral width in the proton dimension was 2298 Hz; the spectral width in the nitrogen dimension was 1250 Hz. Acquisition of the first HSQC spectrum was complete at 48.17 min and the remaining spectra were collected consecutively for 2756 min (28.5 min/acquisition). Additional time points were collected at 3127 and 4399 min. Data were processed by exponential line broadening in $\omega 2$ and a shifted sine bell function in $\omega 1$. Proton and nitrogen resonance assignments were used as reported in the accompanying paper (*29*).

Analysis of Exchange Rates. Cross-peak volumes in each HSQC spectrum were measured by use of Felix 950 (Molecular Simulations, Inc.). These volumes were plotted against the end time of each experiment. Decay curves, representing nonlinear least-squares fits of first-order exponentials to the data points, were generated with KaleidaGraph (Synergy Software) and were used to calculate k_{obs}. Peak volumes were not normalized because the sample was not removed from the spectrometer during data acquisition. By use of previously developed hydrogen exchange theory (*40*, *41*) and assumption of the EX2 exchange limit, the equilibrium constant for the local unfolding reaction, K_{op}, was calculated as k_{obs}/k_3. In this equation, k_{obs} is the exchange rate observed in the current experiments and k_3 is the intrinsic exchange rate for the exposed proton, given the pH, the local sequence, and temperature. Assumption of the EX2 limit is reasonable because exchange in another closely related eukaryotic cytochrome *c* from horse was shown by mass spectrometry to be consistent with the EX2 limit (*26*). k_3 was calculated with the SPHERE program (HXPRED4-6, A. Robertson, P. Laub, Y.-U. Zhang, and H. Roder; http://dino.fold.fccc.edu:8080), which implements previously described methods (refs *42* and *43* and references therein). Log *P* was then calculated as log $(1/K_{op})$. Log *P* is proportional to the free energy change for the local unfolding reaction, $\Delta G_{op} = 2.3\ RT \log P$.

For more accurate comparison of our data to hydrogen exchange data previously published on unlabeled iso-1-cytochrome *c* (*23*), the log *P* values reported by Marmorino et al. were not used directly. Instead, the log *P* values were recalculated using the k_3 values computed by SPHERE (as described above) and the k_{obs} previously reported (*23*). All of these data are reported in Tables S1 and S2 (Supporting Information).

RESULTS AND DISCUSSION

Determination of the Observed Exchange Rates. Of the 108 residues in yeast iso-1-cytochrome *c*, 104 are nonproline residues and have exchangeable backbone amide protons. Most of the residues in both the oxidized and the reduced proteins were distinguishable and assigned in the [^{1}H−^{15}N] HSQC spectrum [see accompanying paper (*29*)]. Hydrogen exchange rates were calculated for many of these protons by exchanging [*U*-^{15}N]C102T into D_2O and collecting [^{1}H−^{15}N] HSQC spectra periodically over a time course of 1385.8 and 4399.0 min for oxidized and reduced C102T, respectively. The HSQC spectrum for C102T protein in each of its oxidation states acquired at the first time point of the exchange experiments is shown in Figure 1.

^{1}H−^{15}N cross-peak volumes were measured from the HSQC spectrum at each time point and plotted as a function

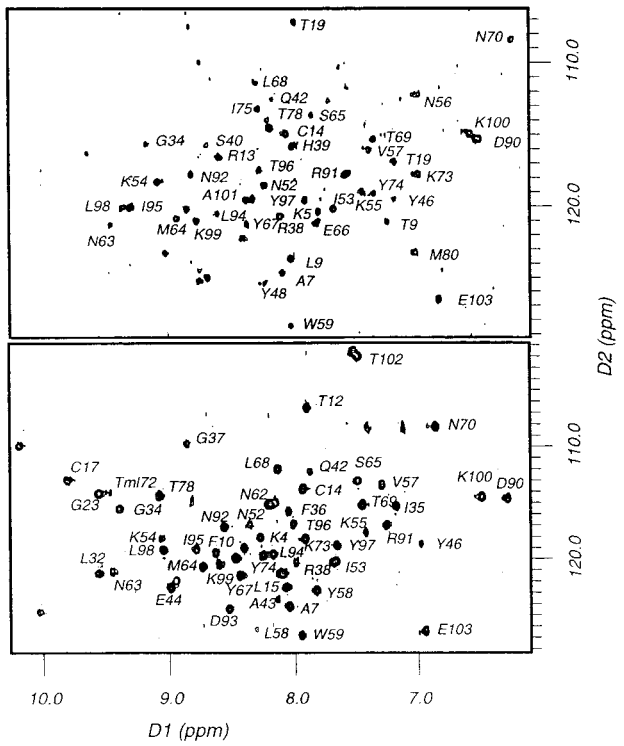

FIGURE 1: HSQC spectra of reduced (top) and oxidized (bottom) [*U*-^{15}N]iso-1-cytochrome *c* (C102T) in D_2O at the first time point in the exchange experiment. The first time point was at 46.85 min for the experiment on oxidized protein and 48.17 min for the experiment on reduced protein. Many of the cross-peaks are labeled with their confirmed assignments. See accompanying paper for the complete set of ^{15}N assignments for C102T in both oxidation states (*29*).

of time. First-order exponentials were fit to the data and observed exchange rates, k_{obs}, were calculated for all assignable and observable residues in both oxidized and reduced proteins (see Materials and Methods). Examples of the decay curves and the fits of the exponentials are shown in Figure 2. The actual values of k_{obs} for the assigned amide protons of oxidized and reduced C102T are presented in Tables S1 and S2.

Exchange Rates Determined from the Current Data. For oxidized [*U*-^{15}N]C102T, 53 resonances are observed in the HSQC spectrum at the first time point. Exchange rates can be directly calculated for 31 of these. For 18 amide resonances (marked as S and S2 in Table S1), the volume decrease was too small to calculate an accurate exchange rate. For four protons, Gln 42, Tyr 46, Lys 55, and trimethyllysine 72 (marked as D2 in Table S1), peak volume could be observed at the first time point, but not thereafter; thus, exchange rates could not be calculated for these amides. Thirty-eight amide resonances (marked as D in Table S1) could not be observed in the first HSQC spectrum at 46.8 min. Resonances for His18 and Asn 31 are outside the spectral window used in these HSQC experiments. Eleven amide resonances remain unassigned in oxidized [*U*-^{15}N]-C102T.

Remarkably, 66 resonances can be observed in the first HSQC spectrum of 48.17 min for reduced [*U*-^{15}N]C102T. Exchange rates can be calculated for 25 of these amide protons. The volume decrease for 20 amide resonances (marked as S or S2 in Table S2) is too small to allow accurate

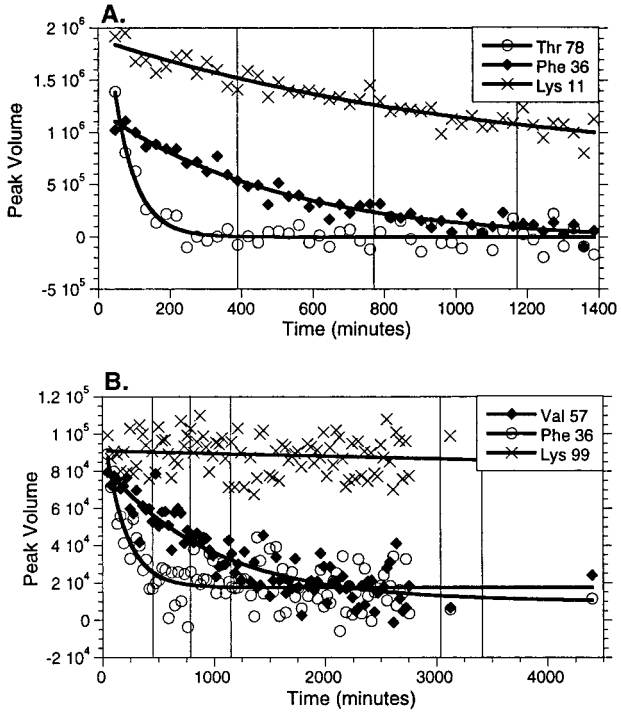

FIGURE 2: Examples of decay curves (amide $^{15}N-H$ cross-peak volumes plotted versus time) for selected protons in oxidized (A) and reduced (B) iso-1-cytochrome *c* (C102T). The cross-peaks shown are Lys 11 (×), Phe 36 (◆), and Thr 78 (○) for oxidized C102T (A) and Lys 99 (×), Val 57 (◆), and Phe 36 (○) for reduced C102T (B). The curves through the data points represent a nonlinear least-squares fit of the volumes to a first-order exponential (see Materials and Methods). The diamond symbols show curves where the rates determined for both labeled and unlabeled C102T are comparable; the × symbols show examples of slower rates where the rate is better determined from the experiments on unlabeled protein; the circle symbols show examples of faster rates where the rate is better determined on labeled protein. For comparison of the experimental time scale, the vertical lines represent the first time points observable in previous hydrogen exchange experiments on unlabeled C102T under essentially identical experimental conditions (*23*).

calculation of exchange rates. Eleven of the protons in the reduced protein are marked as D2 because the amide resonance peak could be observed in the first spectrum but was not observed thereafter, so an exchange rate could not be calculated. The resonance for Asn 31 is outside the spectral window in the HSQC experiments on reduced protein. Ten protons (marked as OL or Br in Table S2) could not be distinguished in the HSQC spectra because of resonance overlap or broadening, and exchange rates could not be calculated for these amides. The amide resonances for Lys 22, Ala 43, Glu 44, and Asp 93 are not well-resolved in the HSQC spectrum and were difficult to assign, so the rates for these amides were determined by comparison to rates that were previously reported (*23*). Only 24 resonances were not observed in the first spectrum and are marked as D in Tables S1 and S2.

Comparison of k_{obs} to Previously Determined Exchange Rates. Complete isotopic labeling of iso-1-cytochrome *c* allowed us to collect spectra and measure exchange rates for protons that exchange more quickly than those previously reported by Marmorino et al. (*23*) for unlabeled C102T. In the current experiments, the first time points collected for oxidized and reduced C102T were 46.85 and 48.17 min, respectively. At this first time point, 53 protons for the oxidized protein and 66 protons for the reduced protein exchanged slowly enough to be observed in at least one spectrum at pH 4.6 and 25 °C (Figure 1). This compares to the 36 and 47 protons observed at the first time point of 6.55 h under essentially identical conditions for unlabeled oxidized and reduced C102T, respectively (*23*).

This rapidity of experiments allowed us to determine rates as fast as 0.02 s^{-1}. This difference is clearly illustrated for Thr 78 in oxidized C102T (Figure 2A) and Phe 36 in reduced C102T (Figure 2B). These protons could not be observed during the experiments on the unlabeled protein (*23*). From the current work on labeled cytochrome *c*, exchange rates for 17 and 5 protons in the oxidized and reduced proteins, respectively, in this shorter time regime can now be calculated (Tables S1 and S2).

However, there is also a longer time range for exchange that was more readily observed in previous experiments done on unlabeled iso-1-cytochrome *c* (*23*). For 15 and 19 protons in the oxidized and reduced proteins, respectively, exchange rates in these longer time frames were not observed in the current experiments because the total time of data collection was short enough that the decay curves were flat or did not decay completely. Protons with rates in this regime are marked as S in Tables S1 and S2. Examples of Lys 11 and Lys 99, oxidized and reduced, respectively, falling into this category are shown in Figure 2. For these protons, the rates determined by Marmorino et al. are used in the subsequent discussion on C102T structure.

There is also a time range where the hydrogen exchange rates can be observed in both the current experiments on [*U*-^{15}N]C102T and in previous experiments on unlabeled C102T, such as Phe 36 in oxidized C102T (Figure 2A) and Val 57 in reduced C102T (Figure 2B). Of these observed rates, about 50% were essentially identical (within experimental error) in both the current and previously reported experiments. For an additional 30%, the rates were comparable but not strictly within the experimental error limits. The remaining exchange rates that were not identical or similar are listed in Table 1, along with the probable reason for the discrepancy. Some of these rates were calculated with data that were on the edge of the time scale for the particular experiment. These include very slowly exchanging protons in the HSQC experiments or more rapidly exchanging protons in the COSY experiments. In some cases, partially overlapped amide resonances in the HSQC spectra may account for some discrepancies in our data, or the overlap of chemical shifts in the fingerprint (Hα−HN) region of the COSY spectra in the data reported by Marmorino et al. (*23*). Furthermore, our use of gradient-based water suppression could account for further gains in signal. In subsequent analysis of protein structure and dynamics (see below), we use the k_{obs} from either the HSQC experiments or the COSY experiments, depending on which rate is expected to be most accurate, in those cases where there is a discrepancy. In those cases where no source of error can be identified, the rate calculated from the HSQC experiments is used. For these cases, the choice of exchange rate is identified in Table 1 by an asterisk.

The exchange rates for a few amide protons, including Phe 10 and Asn 92 in both oxidation states, Tyr 74, Lys 87, and Tyr 97 in oxidized protein, and Leu 15, His 18, Trp 59,

Table 1: Observed Rates for Oxidized and Reduced Iso-1-cytochrome *c* for Which the Exchange Rates Calculated for Labeled and Unlabeled Protein Are Significantly Different[a]

residue	k_{obs} (error, min^{-1}) [*U*-^{15}N]-labeled	k_{obs} (error, min^{-1}) unlabeled	probable reason
	Oxidized Iso-1-cytochrome *c*		
Lys 11	0.009 (±0.0003)	*0.003 (±0.00003)	edge of time resolution (HSQC)
Thr 12	*0.014 (±0.0017)	0.00052 (±0.000017)	
Arg 13	D	*0.0001 ((±0.00005)	OL in HSQC
Cys 17	*0.018 (±0.002)	D2	
Gly 23	*0.00011 (±0.0005)	D	
His 26	*D	D2	OL with F82 in H dimension
Arg 38	0.036 (±0.01)	*0.0011 (±0.00005)	OL in HSQC spectrum
Gln 42	*D2	0.007 (±0.001)	edge of time resolution (COSY)
Ser 47	D	0.0002 (±0.0001)	OL in H dimension
Asn 62	*0.002 (±0.0002)	D	
Asn 70	*0.002 (±0.0002)	D	
Lys 73	*0.0046 (±0.00032)	0.028 (±0.0005)	edge of time resolution (COSY)
Tyr 74	*0.00046 (±0.00026)	D	
Ile 75	*D	0.0002 (±0.00002)	OL in H dimension
Phe 82	*0.016 (±0.002)	D2	
Asp 90	*0.01 (±0.001)	D2	
Asn 92	*343E-05 (±0.0008)	D	OL in H dimension
	Reduced Iso-1-cytochrome *c*		
Lys 27	D	*0.0001 (±0.000033)	weak ^{15}N assignment
Ile 35	D	0.00002(±0.00001)	OL in HSQC spectrum
Phe 36	0.0054 (±0.00091)	0.0030 (±0.00067)	edge of time resolution (COSY)
Gln 42	*D	0.002(±0.001)	OL in H dimension
Ser 47	*D	0.01(±0.00017)	
Glu 66	*0.0014 (±0.00026)	D	
Asn 70	0.00054 (±0.00021)	*0.00083 (±0.000083)	edge of time resolution (HSQC)
Asn 92	*0.00081 (±0.00064)	D	OL in H dimension
Lys 100	*0.0042 (±0.00059)	0.0020 (±0.00067)	edge of time resolution (COSY)

[a] k_{obs} ([*U*-^{15}N]-labeled) are observed exchange rates for [*U*-^{15}N]iso-1-cytochrome *c* (C102T) taken from the data reported in Tables S1 and S2. k_{obs} (unlabeled) are for unlabeled iso-1-cytochrome *c* (C102T) taken from ref 23. An asterisk indicates the rate was chosen as most reliable from the known data. D = denatured; amide proton not visible in first time point. D2 = amide proton visible only in first time point but not thereafter. OL = overlap in chemical shifts in the NMR spectrum.

Thr 69, and Leu 98 in reduced protein, should still be considered as estimates. Some of these amide resonances decayed very slowly and were also presented as estimates in the previous work (*23*). Since the current time scale is shorter, we were not able to calculate exchange rates for these protons. For a few, the cross-peak is obscured or overlapped with another resonance in either the HSQC experiments reported here or the COSY experiments reported previously (*23*) and the exchange rate was reported as an estimate in the work in which a rate was reported. The estimated rate is used in the complete analysis presented here.

Exchange rates could not be determined for Met 64 in both oxidation states and for Lys 11, His 33, and Leu 94 in the reduced protein by either previous or current experiments. Leu 94 exchanges too slowly for decay to be observed by either method. The others were either obscured or not unambiguously assigned in both experiments. By combining the data previously collected on unlabeled C102T with the current data collected on labeled C102T, exchange rates can now be reported for 53 protons in the oxidized state and 52 protons in the reduced state.

Calculation of K_{op} and Log P. The equilibrium constant for the local unfolding reaction, K_{op}, was calculated as k_{obs}/k_3, where k_3 is the intrinsic exchange rate for a given amide proton (calculated as described in Materials and Methods). The protection factor, *P*, is the inverse of K_{op} (K_{op}^{-1}). The free energy for the opening reaction, ΔG_{op}, is thus proportional to log *P*. To analyze this free energy for hydrogen exchange on a residue-by-residue basis throughout the protein, log *P* values were plotted versus residue number (Figure 3). For those protons for which the data on unlabeled protein were used, the log *P* was recalculated using the k_{obs} reported by Marmorino et al. (*23*) and k_3 was calculated here using the SPHERE program (see Materials and Methods).

Hydrogen Exchange and Helix Secondary Structures in C102T. Protection from exchange is due to hydrogen bonding, to burial within the protein, to resistance of surrounding structure to deformation, or to some combination of these factors (*27*). The protons that show protection from exchange and for which we can calculate protection factors clearly show the outline of all secondary structures, including the highly hydrogen-bonded helices and the less hydrogen-bonded loops, in cytochrome *c* in both oxidation states (Figure 3). Overall, the protection factors do not correlate with the overall temperature factors observed in the crystal structures (Figure 3), as has been shown previously in horse cytochrome *c* and hen egg white lysozyme (*27*, *44*).

Protection factors can be calculated for all amide protons in the C-helix (residues 90−103) in both oxidized and reduced states. This would be expected for the residues that pack against the rest of the protein, but even those residues at the solvent-accessible surface of this helix exhibit log *P* values greater than 2.5. These solvent-accessible protons could be partially protected from exchange by the N-terminal extension, which lies across the surface of the C-helix in the crystal structure of C102T (*12*, *31*). However, in solution, the N-terminal extension is rather flexible. No protection factors could be calculated for any amide protons in this

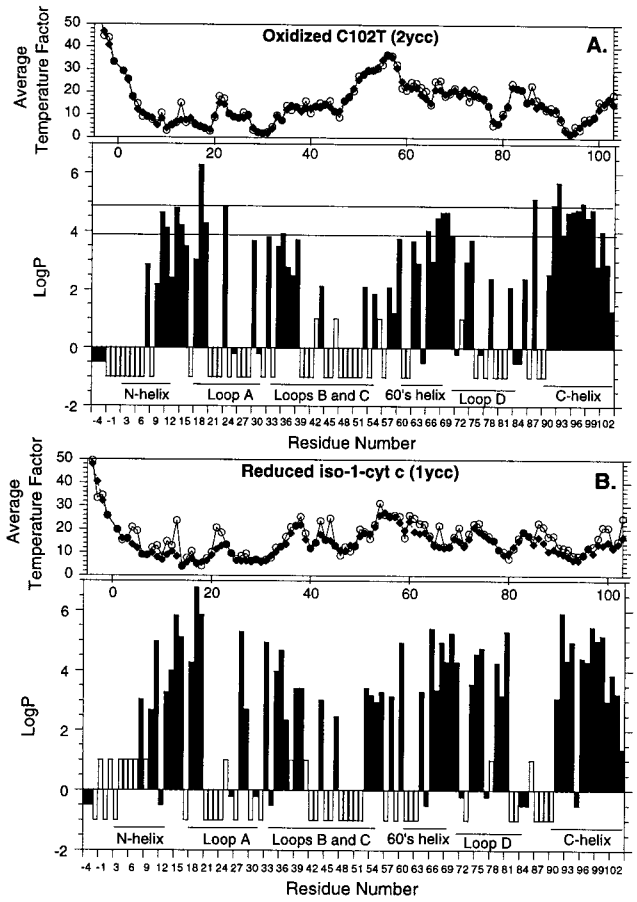

FIGURE 3: Histogram of log *P* versus residue number for the oxidized (A) and reduced (B) proteins. The top of each panel shows the average temperature factors for each residue taken from the crystal structures for oxidized C102T (*31*) and reduced C102 (*12*). Open circles are the average temperature factor for all atoms in the residue, and the solid diamonds are for the backbone atoms only. The log *P* values used in this figure were taken either from the current data on labeled C102T or from the previous data taken on unlabeled protein (*23*) (see Tables S1 and S2). The white bars at 1.0 are those amide protons that exchange rapidly and we see peak volume only in the first time point (D2 in Tables S1 and S2). Exact exchange rates cannot be calculated for these protons. The white bars at −1.0 are those amide protons that have exchanged by the first time point of about 47 min in our experiments and are thus not visible in the HSCQ spectrum (marked as D in Tables S1 and S2). The black bars at −0.5 are either those for which resonance data were insufficient for calculation of an exchange rate or those that remained unassigned by us or in previous work (*23*), so no protection factor can be calculated. Black bars at −0.2 are prolines. Horizontal lines in panel A represent log *P* values that were calculated from the lower and upper limits of ΔG_d for oxidized C102T at 300 K, pH 4.6 (*35*). In panel B, the lower and upper limits of log *P* calculated from ΔG_d for reduced C102T at 300 K, pH 4.6 are 8.02 and 9.04 and are beyond the scale of the graph.

extension in either the oxidized or reduced states (Figure 3)—most protons are gone by the first time point—suggesting that the N-terminal extension probably does not provide much protection to the amide protons in the C-helix. Peptide studies suggest that the C-helix is relatively stable (*45*); thus, the stability of the helix and its component hydrogen bonds could account for the observed protection factors. As demonstrated for this helix previously (*28*), the protection factors decrease at both helix N- and C-termini. This suggests some fraying of the helix ends, as would be predicted by helix−coil transition theory (*46*, *47*); however, the amide protons exchange slowly enough that protection factors can still be calculated for all residues in the helix, even the C-terminal residue Glu 103, which is also the C-terminal residue of the protein.

The amide protons of the N-helix (residues 3−13) are not as uniformly protected from exchange as those in the C-helix (Figure 3). Log *P* values ranging from 3 to 4 can be calculated for amides at the C-terminal end of the N-helix. However, the amide resonances at the N-terminus of the N-helix are either exchanged by the first (oxidized state) or second (reduced state) time point, suggesting significant fraying at the N-terminus of this helix. For instance, the Gly 6 resonance is gone by the first or second time point in both oxidation states. The Gly 6 amide proton is hydrogen-bonded to Ser 2 in the crystal structure (*12*); furthermore, NOE patterns are characteristic of a helical conformation (*29*). Thus, these residues are in a helical conformation, but the *i* to *i* + 4 hydrogen bond, which is expected for a strictly α-helical conformation, does not provide the amide proton with much protection from exchange by deuterium in solution. The amides in the middle of the helix are also not completely protected. For example, the amide proton resonance for Thr 8 is gone by the first (or second) time point, depending on the oxidation state. Furthermore, Leu 9, with log *P* values of 2.91 and 2.68 in the oxidized and reduced states, respectively, exchanges relatively rapidly (within 4 h) for being in the middle of a helix. These results demonstrate little or no protection at the N-helix N-terminus with increasing protection of amide protons toward the C-terminus of this helix. This is similar to exchange behavior observed in horse cytochrome *c* (*27*). In yeast iso-1-cytochrome *c*, which contains an N-terminal extension of five residues adjacent to the N-helix, these data correlate with the recent suggestion that deformability of adjacent structures could cause a faster exchange rate (*27*). Because of the rapidity of exchange, we cannot calculate exchange rates for any of the assigned amide protons in this extension (Tables S1 and S2); furthermore, the first two residues in the N-terminal extension have not been assigned in this work or in previous work on C102T or C102S because interresidue NOEs involving these residues cannot be identified. Thus, this N-terminal extension is largely unstructured in solution and the lack of structure in the N-terminal extension could cause the rapidity of exchange seen at the N-helix N-terminus. In horse cytochrome *c*, exchange rates also cannot be calculated for the first six residues of the N-helix (*27*); however, the explanation for protection is different because this protein lacks the N-terminal extension. We would not expect to see large protection factors for the first three residues of the horse cytochrome *c* N-helix because they are also the first three amides in the protein and would not be hydrogen-bonded to any other atom if the residues are in an α-helical conformation.

The amide protons in the 60s helix exhibit protection factors between 3 and 4, but again, the amide hydrogens in this helix are not as uniformly protected as those found in the C-helix (Figure 3). For example, log *P* values for the amide protons of Asn 62 and Asn 63 are 3.67 and 2.92, as calculated from the HSQC experiments on oxidized protein. In the HSQC experiments on the reduced protein, the log *P* of Asn 63 was determined to be 3.31, while the amide proton resonance of Asn 62 is gone by the first time point. Protection

factors for these residues could not be calculated from the COSY experiments on unlabeled protein (*23*).

Hydrogen Exchange and Loop Structures in C102T. Ω-loops are nonregular secondary structures first described in 1986 (*48*) and described for iso-1-cytochrome *c* in 1989 (*49*). As observed for the helices, the protection factors in loops do not correlate with the temperature factors observed in the crystal structure (Figure 3). As suggested previously (*23*) and now shown in greater detail, a distinctive hydrogen exchange pattern follows the outline of the Ω-loops (Figure 3). In each case, the protection factors are largest at the loop ends and decrease as one moves toward the middle, which is exactly opposite the pattern observed for the helices (Figure 3). Hydrogen bonds observed in the crystal structures do not always correlate with protection factors in these loop structures.

In loop A (residues 18−32), protection factors for residues 18, 19, and 32 at the loop termini are all above 3.5 in both oxidation states. In loop D (residues 70−84), the protection factors for the amide protons of Asn 70 and Phe 82 at the loop ends are above 2.0 in the oxidized state. In the reduced form of the protein, log *P* for the amide proton of Asn 70 is 3.88, while the Phe 82 amide proton is gone by the first time point. The protection of amides at the N-terminus of loop A and the C-terminus of loop D can be explained because the His 18 and Met 80 side chains are ligands to the heme iron. However, this explanation does not account of the protection of amides at the C-terminus of loop A or the N-terminus of loop D. Proximity to, and significant interactions with, the heme group could explain the protection of amides at the C-terminus of loop A, but this explanation does not hold for the N-terminus of loop D. Nor does it account for the observation that amides at the ends of loops B and C are protected from exchange. Overlapping loops B (residues 34−43) and C (residues 40−54) are at the bottom of the heme crevice. As found for the other loops, amide protons at the N- and C-termini of these loops, specifically Gly 34, Ala 43, and Lys 54, exhibit protection factors above 3.0 and 1.8 in the reduced and oxidized forms, respectively (Figure 3, Tables S1 and S2). These residues are farther than the average residue from the heme.

Another factor that could account for enhanced protection of loop ends is the turn of helix found at the N-terminal of loop D and the C-terminal of loop C. This could account for the protection of Asn 70. However, neither the proximity to heme nor the helical turns explains the protection of Gly 43, Ala 43, or Lys54.

However, while amide protons at the Ω-loop ends clearly exhibit relatively large protection factors, the pattern for the overall structures is quite different from that observed in the helices. In loops, protection factors cannot be calculated for a number of residues in the middle of each loop because the amide resonance is absent in either the first or second time point in the HSQC experiments. As an example, Figure 4 identifies those residues for which the amide proton is exchanged by the first time point of 46 min in labeled, oxidized C102T. In every case, protection factors for the amide protons in the middle of the loop cannot be observed. In other proteins, it might be argued that the protection factors found at the loop ends are due to the fact that loop ends are normally found adjacent to regular secondary structures, helices and strands. However, this argument cannot be made for cytochrome *c*, as the loop ends are not found at the termini of regular secondary structures.

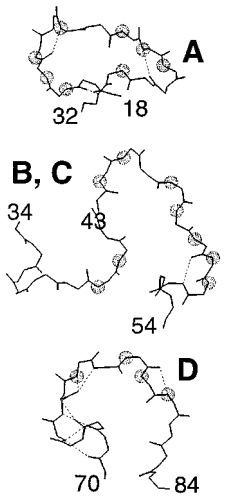

FIGURE 4: Backbone models of the loop structures in C102T show how the loop ends are protected from hydrogen exchange but the loop middles are not. The loop structures shown are loop A, residues 18−32; loops B and C, residues 34−54, and loop D, residues 70−84. The amides whose protons are not visible at the first time point (46 min) are indicated by small spheres. Data are shown for the oxidized protein. As shown, the structures represent the substructures of the RYGB model described by Englander and co-workers (*24*, *25*): substructure II contains loop A as well as the 60s helix, substructure III corresponds to loops B and C, and substructure IV is loop D. The structures were taken from 2ycc, the structure for oxidized C102T (*31*). Models were constructed with InsightII (MSI).

Although the correlation between hydrogen bonds and protection factors is clear in the helices, the protection factors do not clearly correlate with hydrogen bonding in the loop regions. Of the 30 backbone−backbone hydrogen bonds observed in the solution structure of reduced C102S (*17*), four exchange too quickly for exchange rates to be calculated: Gly 24, Ile 35, Gly 37, and Phe 82. All of these residues are in loop regions. The amide protons of loop residues Gly 34, Ala 43, and Lys 54 exhibit protection factors in both oxidation states. In the crystal structures 1ycc and 2ycc (*12*, *31*), the Gly 34 amide is hydrogen-bonded to the carbonyl oxygen of Cys102 in both oxidation states. The amide of Asn 70 is hydrogen-bonded to the Tyr 67 carbonyl oxygen in the reduced, but not oxidized, crystal structure, while the Ala 43 amide is hydrogen-bonded to the Tyr 48 side-chain hydroxyl in the oxidized, but not the reduced, protein. Surprisingly, the Lys 54 amide is at the surface and is not hydrogen-bonded to any other atom in crystal structures of either oxidation state. Thus, the correlation between hydrogen bonding and protection factors is not consistent in these loop structures.

Comparison to the Solution Structures of C102S Iso-1-cytochrome c. The overall solution structure of the unlabeled C102S variant of iso-1-cytochrome *c* at pH 7.0 was found to be quite similar to the crystal structure (*17*, *19*). These researchers also reported hydrogen exchange data by obtaining NOESY spectra 0, 1, 2, and 6 days after exchange into D_2O. While rates could not be calculated from this limited data set, those protons still present after 6 days in D_2O could be observed. Of the 27 amide−α-proton resonances that were still present in oxidized C102S after 6 days in D_2O, 14 were found in loop regions (*19*). Of the 47 amide−α-proton

resonances present in reduced C102S after 6 days, 28 were in loop regions (*17*). Thus, these researchers found protected amides in both loops and helices. This general feature of hydrogen exchange behavior is thus supported by previous work on unlabeled C102T at pH 4.6 and C102S at pH 7.0 and the more detailed data from [*U*-^{15}N]C102T at pH 4.6 presented here.

However, the list of slowly exchanging amide protons obtained from the experiments on unlabeled C102S is different from the list obtained from experiments done on both labeled and unlabeled C102T. Of the 27 amide proton resonances in the oxidized protein listed as slowly exchanging by Banci et al. (*19*), 12 were found to be rapidly exchanging in the current work, including Ala −1, Gly 6, Thr 8, Lys 27, Asn 31, His 33, Ala 43, Glu 44, Ala 51, Lys 54, Asp 60, and Thr 78. Likewise, in the reduced protein, 11 protons listed by Baistrocchi et al. (*17*) as slow exchangers were gone by the first time point in the current work. This list includes Thr 8, Gln 16, Lys 22, Gly 23, Gly 24, Ser 40, Tyr 48, Thr 49, Ala 51, Phe 82, and Lys 89. These differences are profound because the slowly exchanging protons observed in the Banci and Baistrocchi work were still present after 6 days, while these same protons are exchanged by 46 or 48 min in the work presented here. Furthermore, the protons exhibiting differences are scattered throughout the protein structure.

What is the explanation for these significant differences? For these resonances, the results reported here on [*U*-^{15}N]-C102T are in very good agreement with the experiments previously reported on unlabeled C102T (*23*), providing confirmation that the calculated rates and protection factors are consistent and correct for this variant and under these conditions. One difference between the two sets of experiments is that the current data and the previous work were acquired on the C102T variant, while Banci and Baistrocchi and co-workers observed hydrogen exchange on the C102S variant of iso-1-cytochrome *c*. Experiments on the wild-type C102 protein and the C102T variant suggest that mutations at residue 102 have little effect on the structure or stability of the protein (*12*, *31*, *35*, *50*, *51*). In fact, the crystal structures of C102T and WT iso-1-cytochrome *c* are very similar (*31*) and detailed thermal denaturation studies show that the properties of C102T and C102S are essentially identical (*52*). The C102T, C102S, and C102A variants are used as "wild type" by various groups, again working under the assumption that mutations at position 102 do not affect the overall structure or stability of the protein. It seems unlikely that a change at position 102 would have such a wide influence on exchange rates throughout the protein.

The second difference between the experiments on C102S and those on C102T (both current experiments and those of Marmorino et al.) involves the solution conditions. C102T data were collected on protein dissolved in 50 mM acetate buffer, pH 4.6, at 298 K. The C102S hydrogen exchange data were collected on protein dissolved in 50 mM phosphate buffer, pH 7.0. Both buffers and pH are different. Binding of multivalent anions in the phosphate buffer might have distinct local effects on exchange. The pH difference should also have a significant effect on the intrinsic hydrogen exchange rates. At higher pH, the concentration of hydroxide ions in solution is increased and thus the exchange rate should increase, not decrease, due to an increase in base catalysis (*53*). However, if the change in pH significantly changed the structure of the protein, then the exchange rates might change. Comparison of the proton chemical shifts used in this study to those done on C102T at pH 7.0 (*50*) shows that the shifts are virtually identical, suggesting little change in the overall structure of this protein with change in pH.

Another possibility that might explain the differences in exchange rates in the C102T and C102S experiments is that the protein at pH 4.6 might be starting to show some changes in dynamic behavior because the protein is closer to the low pH unfolding transition. Cohen and Pielak have studied the pH-dependent behavior of C102T (*35*). They show that the thermal denaturation temperature of C102T decreases steadily from 55.3 °C at pH 5.0, to 52.6 °C at pH 4.6, to 49.7 °C at pH 4.3. ΔG_D also shows a gradual decrease with pH, from 5.1 kcal/mol at pH 4.6 to close to 0 at pH 3.0 (*35*). Thus, lowering the pH may cause the observed increase in exchange rates for certain protons if certain regions of the protein were preferentially destabilized.

A final possibility might be the effect of pH on heme ligand states. At pH 4.6, the heme in about 5% of the folded, oxidized protein will exist in the high-spin form, while 30% will be high-spin in the unfolded state. At pH 7, essentially all hemes will be in the low-spin state. The differences in the heme spin state and the resulting differences in ligands could affect the hydrogen exchange properties. Only a detailed study of the pH dependence of hydrogen exchange in yeast iso-1-cytochrome *c* can answer this intriguing question.

Differences in Hydrogen Exchange between the Oxidized and Reduced States. Using the combined results of the current exchange experiments and those of Marmorino et al. (*23*), we have been able to compare more completely the differences between the protection factors calculated for amide protons in the oxidized and reduced states of the protein (Figure 5). As previously observed, the difference, $\log P_{ox} - \log P_{red}$, is negative for most residues in the protein, which reflects the greater stability of reduced C102T over oxidized C102T (*54*). The current data also show that the difference in stability between oxidized and reduced C102T is not limited to one region of the protein but is spread over all secondary structures in the protein (Figure 5). This is in agreement with the previous work on unlabeled C102T and C102S (*17*, *19*, *23*).

However, there are a few notable exceptions to the general rule of larger protection factors in the reduced state. In particular, the amides of Gly 23, Gly 29, Gly 37, Leu 58, Asn 62, Phe 82, Leu 85, and Lys 87 show significant protection factors only in the oxidized state (Figure 5). In the reduced state, these residues are exchanged by the first or second time point. A small number of residues, including Arg 13, Phe 36, Phe 38, Leu 68, Asn 92, Ile 95, and Thr 96, exhibit rates that can be measured in both states, but protection in the oxidized state is larger than that in the reduced state (Figure 5). Of these 15 residues, almost half (Arg 13, Gly 23, Gly 29, Gly 37, Phe 82, Leu 85, and Lys 87) are invariant or strictly conserved in 106 eukaryotic cytochromes *c* (*22*). The observations that these residues exhibit exchange behavior that is opposite of that observed for most residues and that they are so very conserved from human to fungal cytochromes *c* would suggest that these residues might undergo an important conformational change

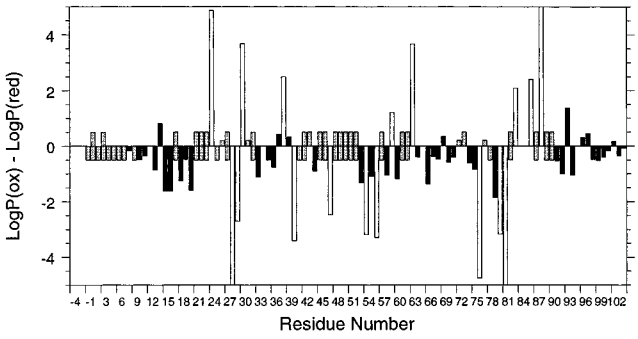

FIGURE 5: Histogram of the difference between the log *P* values for oxidized and reduced C102T versus residue number. Black bars are for those residues where log *P* values could be calculated in both oxidation states; the difference (log P_{ox} − log P_{red}) is plotted. White bars indicate those residues where log *P* could be calculated in only one oxidation state because the amide resonance was gone by the first time point (D) in the other oxidation state. A gray bar at 0.5 only indicates that the resonance peak was gone by the first time point in the reduced state (D) or was gone by the second time point in the oxidized state (D2). Likewise, a gray bar at −0.5 indicates that the resonance peak was gone by the first time point in the oxidized state (D) or was gone by the second time point in the reduced state (D2). A gray bar at both 0.5 and −0.5 indicates that that residue was gone by the first time point (D) in both oxidation states. Gray bars at 0.2 are prolines. No bar indicates lack of data (unassigned resonance peak or overlap of peaks) for one state or the other.

between the oxidized and reduced states. Indeed, mutations at Phe 82 have been found to have a significant effect on the protein function in vivo (*55, 56*), despite little change in the reduction potentials with mutations at this position (*57*).

Comparison of Log P and the Free Energy of Denaturation of C102T. At pH 4.6 and 300 K, the ΔG_d of oxidized C102T has been reported as 5.1 ± 0.3 kcal/mol (*35*). At pH 4.6 and 298 K, ΔG_d of oxidized C102T was determined to be 5.2−6.5 kcal/mol (*23*). Horizontal lines are drawn in Figure 3A representing the log *P* values calculated from ΔG_d for C102T. Our data show that the ΔG_{op} of His 18, Lys 87, Arg 91, Asn 92, and Tyr 97 are higher than the limit of the overall free energy of denaturation of oxidized C102T. Of these, Lys 87, Arg 91, and Tyr 92 in the C-helix are only slightly higher, within or close to the experimental error. Only His 18 and Asn 92 are significantly above the ΔG_d limit. The side chain of His18 is the fifth heme ligand. This side chain remains liganded to the heme, even under denaturing conditions of 4.4 M guanidine hydrochloride, pH 4.7 (*58*). Previous studies did not find Asn 92 to have large log *P* values, which is very different from what we report here. As previously discussed (*28*), the proton chemical shift for this amide proton overlaps another amide proton in the proton dimension, which likely affects the reported rate. In the current experiments, the large ΔG_{op} calculated for this residue should be regarded as approximate because it decayed too slowly for us to see the complete exchange during the time course of our experiments. Thus, the only residue that certainly exhibits a higher ΔG_{op} than the ΔG_d is His 18, an observation than can be rationalized by the experimental evidence described above.

By use of circular dichroism spectroscopy and differential scanning calorimetry, the ΔG_d of reduced C102T at pH 4.6 and 300 K has been directly measured as 11.7 ± 0.7 kcal/mol (*54*). The log *P* values calculated from these numbers are higher (8.02−9.04) than the log *P* values determined for any of the protons in reduced C102T (Figure 3B). Thus, the free energy of reduced, denatured C102T is significantly higher than any of the high-energy native forms that can be detected by hydrogen exchange. Under oxidizing conditions, as soon as the Met 80 or His 18 heme ligands are released, the protein is likely to become oxidized. It is possible that the higher energy states for the reduced protein are invisible to detection by NMR simply because the protein molecules become oxidized by residual O_2 when these conformations are sampled during the experiment. To address these concerns, the reduced sample was reduced with dithionite, the buffers contained fresh ascorbate, and the sample tube was sealed under nitrogen; thus, a reducing atmosphere was maintained and the amount of oxygen exposed to the sample was kept to a minimum throughout the experiments. Furthermore, one would expect that the much longer experimental times reported by Marmorino et al. would accentuate the effect of oxidized, unfolded protein populations, resulting in relatively smaller protection factors calculated from their experiments on reduced protein. However, the protection factors calculated by Marmorino et al., using long experimental times, and those reported here, using shorter experimental times, are comparable (Tables S1 and S2).

Comparison of Log P and the Stability of the Met 80−Fe Bond. Englander and co-workers have previously suggested a substructure (RYGB) model for the structure of oxidized eukaryotic cytochrome *c* (*24, 25*). In this model, substructure I contains the N- and C-helices. Substructure II contains Ω-loop A and the 60s helix. Substructure III contains loops B and C, while substructure IV consists of Ω-loop D. Our log *P* values can be used to delineate these substructures in C102T. The outlines of the secondary structures are clearly visible in the plots of log *P* versus residue number (Figure 3).

Relative to these substructure studies, the difference in the binding affinity between methionine and reduced and oxidized heme iron was recently measured in a model system consisting of blocked methionine and a cytochrome *c* fragment called microperoxidase 11 (*59*). The methionine affinity for the reduced iron was found to be more stable by 3.2 kcal/mol compared to the affinity for the oxidized heme. These workers then showed that $\Delta\Delta G_{op}$ between reduced and oxidized protein for substructure IV, loop D, is also 3.2 kcal/mol. Assuming that the methionine 80−heme ligand would have the same binding affinity in yeast cytochrome *c*, we looked at log *P* values determined here for Ile 75, the marker proton used by Englander and co-workers for large unfolding events in substructure IV (*59*). Interestingly, the increase in log *P* upon reduction for Ile 75 in C102T is only 1.22, corresponding to a free energy change of 1.6 kcal/mol (Figure 5). The free energy change for the neighboring Tyr 74 is even less, with a $\Delta\Delta G_{op}$ of 1.0 kcal/mol. This observation might suggest that local structural fluctuations in C102T are more prevalent than they are in horse cytochrome *c*, thus allowing the protons to exchange without the large substructure unfolding event observed for some protons in the horse protein. Alternatively, it might suggest that Ile 75 does not play the same structural role as a marker proton in C102T as it does in horse heart cytochrome *c*. However, the structures of loop D (substructure IV) in the two proteins are essentially identical with 13 out of 15

identical residues. Further understanding of the underlying differences in stability and folding of cytochrome *c* molecules awaits complete analysis of the hydrogen exchange behavior of C102T in low concentrations of denaturant.

Implications for the Substructure Model of Cytochrome c Folding. Englander and co-workers have also reported that the relative order of stability of the substructures in horse cytochrome *c* is I > II > III > IV; further, they suggest the same order for the folding of cytochrome *c* from the most stable to the least stable substructures: I → II → III → IV. Banci et al. (*19*) reported that their HX data on C102S support this model because the loop A and D regions have "greater flexibility." This statement is based on the assumption that rapid hydrogen exchange correlates with structural fluctuations (*19*). Recently, Milne et al. (*27*) have suggested that rapid hydrogen exchange also correlates with lack of resistance to the motion of adjacent structures, an assertion supported by the hydrogen exchange behavior reported here (see discussion of N-helix and N-terminal extension above).

While the substructures themselves are clearly delineated in the plots of protection factors versus residue number, the interpretation of the relative stability or flexibility of these substructures is not so clear-cut. In oxidized C102T, the substructure with the largest number of most rapidly exchanging protons overall is substructure III, the loop B/C region (Figure 4), in which 10 out of 20 amide protons exchange out by 46 min. This is followed by the loop A region, in which 7 out of 12 amide protons exchange out in 46 min (Figure 4). In both cases, about half the amide protons have exchanged out by the first time point in our experiments. If we reason that the most rapidly exchanging protons will be found in the regions of the protein with the largest structural fluctuations or with the most distortable structure, then we would conclude that loops B/C (substructure III) would exhibit the largest fluctuations, followed by loop A (part of substructure II). This supposition is supported by our ^{15}N relaxation data, where we also find R_{ex} terms, which are indicative of some chemical exchange process on the micro- or millisecond time scale (*29*), in the loop B/C substructure. R_{ex} terms are not observed for the amides in the loop A or D regions.

At this time, we cannot equate the current data to the relative folding of the substructures, as our data were collected under native conditions only. However, the data presented here would suggest that more complete coverage of the secondary structures, particularly the loops, is required to validate the substructure model of cytochrome *c* folding. Most of the loop protons that support the RYGB model are located at the loop ends (*24, 25*). As we have clearly shown here, the behavior of the loop ends is different from that of the middle part of the loop. While it is quite possible that loop structure ends and middles will exhibit similar stability data results, as found for the helices, the assertion must be tested. Although it might be difficult to obtain such data by NMR techniques on unlabeled protein, new experiments on [*U*-^{15}N]-labeled protein can now be done with the procedures described here and in the accompanying paper (*29*). Furthermore, the recently developed techniques of stopped-flow and rapid-flow electron paramagnetic resonance (EPR) applied to site-specifically labeled cytochrome *c* might provide some answers (*10*).

Conclusions. We have shown here that we can use [*U*-^{15}N]-iso-1-cytochrome *c* to determine amide exchange rates, even for relatively rapidly exchanging protons. By combining previous exchange data on unlabeled protein with the current data, we can calculate exchange rates for significantly more protons than could be determined in the unlabeled protein, particularly in the oxidized state. These data allow us to confirm the previous data and resolve some ambiguities. Some of the data on C102T are inconsistent with data collected on the C102S variant, suggesting pH-dependent dynamic changes in the protein that are reflected in the exchange rates. The hydrogen exchange behavior outlines the secondary structures of cytochrome *c*, with different patterns of behavior observed for the helices and loops.

ACKNOWLEDGMENT

We thank Ms. Lynn McNaughton for assistance during NMR data acquisition and Mr. Terry Boose for protein purification and technical assistance with some of these experiments. We acknowledge the Wadsworth Center for support of the NMR Structural Biology Facility. J.S.F. thanks Molecular Simulations, Inc., for hardware support during her sabbatical.

SUPPORTING INFORMATION AVAILABLE

Two tables containing the exchange rates, k_{ex} values, and log *P* values for both oxidized and reduced yeast iso-1-cytochrome *c* (C102T) at 25 °C, pH 4.6. This material is available free of charge via the internet at http://pubs.acs.org.

REFERENCES

1. Pettigrew, G. W., and Moore, G. R. (1987) *Cytochromes c Biological Aspects*, Springer-Verlag, Berlin.
2. Nall, B. T., and Landers, T. A. (1981) *Biochemistry 20*, 5403−5410.
3. Elöve, G. A., Bhuyan, A. K., and Roder, H. (1994) *Biochemistry 33*, 6925−6935.
4. Ramdas, L., Sherman, F., and Nall, B. T. (1986) *Biochemistry 25*, 6952−6958.
5. Sosnick, T. R., Mayne, L., and Englander, S. W. (1996) *Proteins: Struct., Funct., Genet. 24*, 413−426.
6. Pierce, M. M., and Nall, B. T. (1997) *Protein Sci. 6*, 618−627.
7. Shastry, M. C. R., and Roder, H. (1998) *Nat. Struct. Biol. 5*, 385−392.
8. Pryse, K. M., Bruckman, T. G., Maxfield, B. W., and Elson, E. L. (1992) *Biochemistry 31*, 5127−5136.
9. Roder, H., Elove, G. A., and Englander, S. W. (1988) *Nature 335*, 700−704.
10. Qu, K., Vaughn, J. L., Sienkiewicz, A., Scholes, C. P., and Fetrow, J. S. (1997) *Biochemistry 36*, 2884−2897.
11. Bushnell, G. W., Louie, G. V., and Brayer, G. D. (1990) *J. Mol. Biol. 214*, 585−595.
12. Louie, G. V., and Brayer, G. D. (1990) *J. Mol. Biol. 214*, 527−555.
13. Ochi, H., Hata, V., Tanaka, N., Kakudo, M., Sakurai, T., Aihara, S., and Morita, Y. (1983) *J. Mol. Biol. 166*, 407−418.
14. Takano, T., and Dickerson, R. E. (1981) *J. Mol. Biol. 153*, 79−94.
15. Tanaka, N., Yamane, T., Tsukihara, T., Ashida, T., and Kakudo, M. (1975) *J. Biochem. (Tokyo) 77*, 147.
16. Qi, P. X., DiStefano, D. L., and Wand, A. J. (1994) *Biochemistry 33*, 6408−6417.
17. Baistrocchi, P., Banci, L., Vertini, I., Turano, P., Bren, K. L., and Gray, H. B. (1996) *Biochemistry 35*, 13788−13796.

18. Banci, L., Bertini, I., Gray, H. B., Luchinat, C., Reddig, T., Rosato, A., and Turano, P. (1997) *Biochemistry 36*, 9867−9877.
19. Banci, L., Bertini, I., Bren, K. L., Gray, H. B., Sompornpisut, P., and Turano, P. (1997) *Biochemistry 36*, 8992−9001.
20. Banci, L., Bertini, I., Bren, K. L., Gray, H. B., Sompornpisut, P., and Turano, P. (1995) *Biochemistry 34*, 11385−11398.
21. Qi, P. X., Beckman, R. A., and Wand, A. J. (1996) *Biochemistry 35*, 12275−12286.
22. Moore, G. R., and Pettigrew, G. W. (1990) *Cytochromes c. Evolutionary, Structural and Physicochemical Aspects*, Springer-Verlag, Berlin.
23. Marmorino, J. L., Auld, D. S., Betz, S. F., Doyle, D. F., Young, G. B., and Pielak, G. J. (1993) *Protein Sci. 2*, 1966−1974.
24. Bai, Y., Sosnick, T. R., Mayne, L., and Englander, S. W. (1995) *Science 269*, 192−197.
25. Bai, Y., and Englander, S. W. (1996) *Proteins: Struct., Funct., Genet. 24*, 145−151.
26. Zhang, Z., and Smith, D. L. (1993) *Protein Sci. 2*, 522−531.
27. Milne, J. S., Mayne, L., Roder, H., Wand, A. J., and Englander, S. W. (1998) *Protein Sci. 7*, 739−745.
28. Baxter, S. M., Boose, T. L., and Fetrow, J. S. (1997) *J. Am. Chem. Soc. 119*, 9899−9900.
29. Fetrow, J. S., and Baxter, S. M. (1999) *Biochemistry 38*, 4480−4492.
30. Mulligan-Pullyblank, P., Spitzer, J. S., Gilden, B. M., and Fetrow, J. S. (1996) *J. Biol. Chem. 271*, 8633−8645.
31. Berghuis, A. M., and Brayer, G. D. (1992) *J. Mol. Biol. 223*, 959−976.
32. Cutler, R. L., Pielak, G. J., Mauk, A. G., and Smith, M. (1987) *Protein Eng. 1*, 95−99.
33. Fetrow, J. S., Horner, S. R., Oehrl, W., Schaak, D. L., Boose, T. L., and Burton, R. E. (1997) *Protein Sci. 6*, 195−208.
34. Gao, Y., Boyd, J., Williams, R. J. P., and Pielak, G. J. (1990) *Biochemistry 29*, 6994−7003.
35. Cohen, D. S., and Pielak, G. J. (1994) *Protein Sci. 3*, 1253−1260.
36. Sherman, F., Stewart, J. W., Parker, J. H., Inhaber, E., Shipman, N. A., Putterman, G. J., Gardishy, R. L., and Margoliash, E. (1968) *J. Biol. Chem. 243*, 5446−5456.
37. Margoliash, E., and Frohwirt, N. (1959) *Biochem. J. 71*, 570−572.
38. Hilgen-Willis, S. (1993) Ph.D. Thesis, University of North Carolina, Chapel Hill, NC.
39. Sklenár, V., Piotto, M., Leppic, R., and Saudek, V. (1993) *J. Magn. Reson. 102*, 241−245.
40. Linderstrom-Lang, K. U. (1958) *Deuterium exchange and protein structure*, Methuen, London.
41. Hvidt, A., and Nielsen, S. O. (1966) *Adv. Protein Chem. 21*, 287−386.
42. Bai, Y., Milne, J. S., Mayne, L., and Englander, S. W. (1993) *Proteins: Struct., Funct., Genet. 17*, 75−86.
43. Connelly, G. P., Bai, Y., Jeng, M. F., Mayne, L., and Englander, S. W. (1993) *Proteins: Struct., Funct., Genet. 17*, 87−92.
44. Radford, S. E., Buck, M., Topping, K. D., Dobson, C. M., and Evans, P. A. (1992) *Proteins: Struct., Funct., Genet. 14*, 237−248.
45. Wu, L. C., Laub, P. B., Elove, G. A., Carey, J., and Roder, H. (1993) *Biochemistry 32*, 10271−10276.
46. Zimm, B. H., and Bragg, J. K. (1959) *J. Chem. Phys. 31*, 526−535.
47. Lifson, S., and Roig, A. (1961) *J. Chem. Phys. 34*, 1963−1974.
48. Leszczynski, J. F., and Rose, G. D. (1986) *Science 234*, 849−855.
49. Fetrow, J. S., Cardillo, T. S., and Sherman, F. (1989) *Proteins: Struct., Funct., Genet. 6*, 372−381.
50. Gao, Y., Boyd, J., Pielak, G. J., and Williams, R. J. P. (1991) *Biochemistry 30*, 1928−1934.
51. Sukits, S. F., Erman, J. E., and Satterlee, J. D. (1997) *Biochemistry 36*, 5251−5259.
52. Herrmann, L. M., and Bowler, B. E. (1997) *Protein Sci. 6*, 657−665.
53. Wuthrich, K. (1986) *NMR of proteins and nucleic acids*, John Wiley and Sons, New York.
54. Cohen, D. S., and Pielak, G. J. (1995) *J. Am. Chem. Soc. 117*, 1675−1677.
55. Inglis, S. C., Guillemette, J. G., Johnson, J. A., and Smith, M. (1991) *Protein Eng. 4*, 569−574.
56. Hilgen, S. E., and Pielak, G. J. (1991) *Protein Eng. 4*, 575−578.
57. Lo, T. P., Guillemette, J. G., Louie, G. V., Smith, M., and Brayer, G. D. (1995) *Biochemistry 34*, 163−171.
58. Takahashi, S., Yeh, S.-R., Das, T. K., Chan, C.-K., Gottfried, D. S., and Rousseau, D. L. (1997) *Nat. Struct. Biol. 4*, 44−50.
59. Xu, Y., Mayne, L., and Englander, S. W. (1998) *Nat. Struct. Biol. 5*, 774−778.

BI982742Z